ACS APPLIED MATERIALS & INTERFACES

Letter

www.acsami.org

Experimental and Theoretical Studies on the Effects of Magnetic Fields on the Arrangement of Surface Spins and the Catalytic Activity of Pd Nanoparticles

Ran Li,[†] Yang Yang,[†] Ren Li, and Qianwang Chen*

Hefei National Laboratory for Physical Sciences at Microscale and Department of Materials Science & Engineering, CAS High Magnetic Field Laboratory, University of Science and Technology of China (USTC), Hefei 230026, China

Supporting Information

ABSTRACT: Nanocatalysts have very high catalytic activities due to surface atoms with their unpaired spins. It is the purpose of this paper to investigate the effect of magnetic fields (MFs) on the arrangement of surface spins and their catalytic activities. Pd nanoparticles supported on MIL-100(Cr) were selected as catalysts for the reduction of 4-nitrophenol under MFs. The result demonstrates that MFs can reduce the reaction time from 2.6 to 1.4 min under 0.5 T. This study first shows that the configuration of surface spins has an effect on the catalytic activity, which can be regulated by a foreign MF.

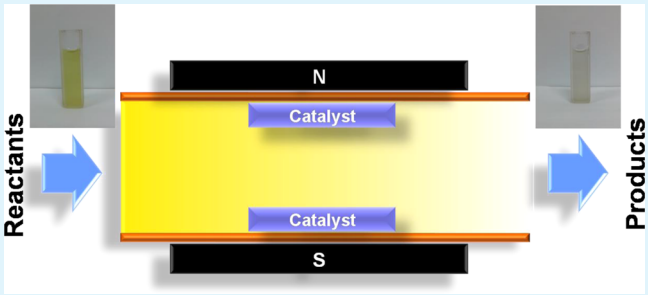

KEYWORDS: *nanocatalysts, Pd nanoparticles, surface spins, magnetic fields, 4-nitrophenol*

Nanocatalysis is becoming a strategic field of science because of its unique charm in the condensation,[1] hydrogenation,[2] carbon−carbon coupling reaction,[3,4] alcohol oxidation,[5] reduction of 4-nitrophenol (4-NP),[6,7] and so on.[8] Currently, great efforts have been made in improving the catalytic performance of nanocatalysts (NCs) with high efficiency, specific selectivity, and good recyclability.[9,10] Great successes have been achieved by tuning the size and shape of NCs.[11,12] For example, Han et al. prepared Pd catalysts with different particle sizes and found that reducing of the Pd particle size led to an increase in the reactivity, selectivity, and apparent activation energy.[13] In addition, it was reported that the high-index facets of Pt nanoparticles (NPs) can provide a greater density of reactive sites than typical Pt NPs.[14]

Indeed, NPs with either small particle size or high-index facets possess a large proportion of surface atoms with respect to bulk counterparts. It was reported that when the size of the NPs decreased from 10 to 1 nm, the surface atoms with a serious shortage of coordination numbers increased from 20% to 90%.[15] These surface atoms will contribute randomly oriented uncompensated surface spins; if these spins can be manipulated, the adsorption characteristics of the surface sites can also be controlled, which would change the catalytic activity of the NCs. Teranishi et al. reported that the *g* values of Pd NPs with a mean diameter of 2.5 nm were about 2.0, implying the paramagnetism of these Pd NPs, different from nonmagnetic polarization in a bulk metallic state.[16] Our group ever systematically studied the influence of magnetic fields (MFs) on the surface energy of Co_3O_4 NPs.[17] When the surface-spin configuration of Co_3O_4 NPs changed from paramagnetic to ferromagnetic, the energy of one (100) and two periodic slab model (111)#1 and (111)#2 surfaces varied from 1.849, 1.645, and 1.638 to 1.326, 1.429, and 1.447 J m^{-2}, respectively. It can be seen that the spin arrangements from disordered to ordered under the induction of MFs lead directly to variation of the surface energy. We, therefore, suggest that variation of the surface energy is able to change the adsorption of the reactants, thus influencing the catalytic activity of NPs. MFs will be developed as a tool to affect the chemical reaction rates if the activity of NCs can be effectively regulated by MFs. Then we can make a chemical reaction slow down or speed up by altering the strength of the MF, which is highly valuable in the chemical industry.

However, hitherto reports about the effect of MFs on the catalytic activity of NCs remain rarely seen, and relevant theoretical work is also scarce. Pd NPs are difficult to oxidize and easily form small steady NPs with large numbers of surface spins, which will be helpful for the study about the effect of MFs on the catalytic activity of NCs. In this paper, liquid-phase reduction of 4-NP to 4-aminophenol (4-AP) by $NaBH_4$ is chosen as the model reaction system, and Pd NPs supported on MIL-100(Cr)[26] (MIL is the abbreviation of "Materials of Institut Lavoisier") were used as catalysts for this study.

The powder XRD patterns of MIL-100(Cr) (i) and Pd/MIL-100(Cr) (ii) are shown (Figure S1 in the SI). Their XRD patterns are almost identical, and no obvious Pd peaks can be seen in Figure S1(ii) in the SI. Inductively coupled plasma measurement shows that Pd loading is only 2.6%. Figure S2 in

Received: December 31, 2014
Accepted: March 6, 2015
Published: March 6, 2015

DOI: 10.1021/am509218a
ACS Appl. Mater. Interfaces 2015, 7, 6019−6024

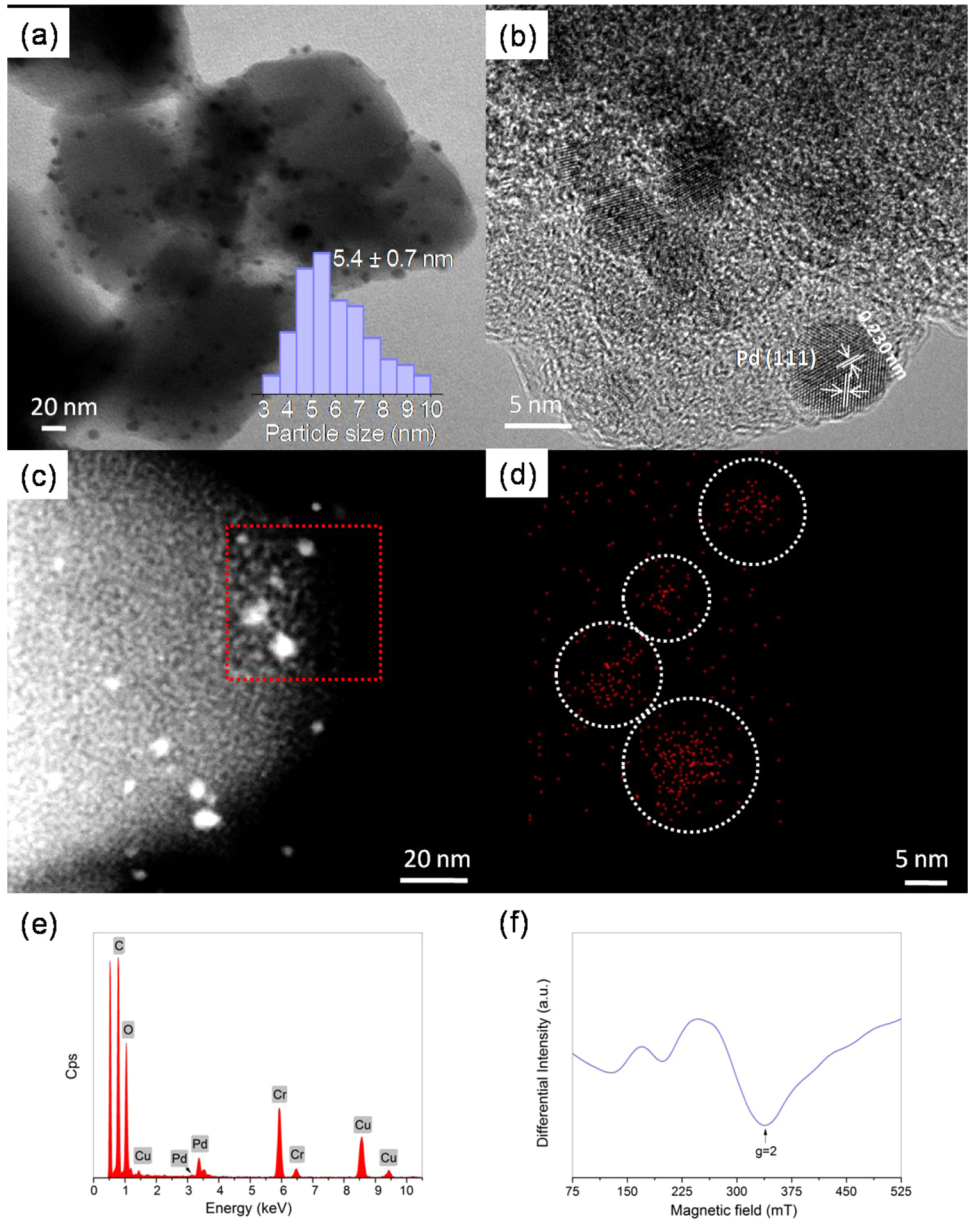

Figure 1. (a) TEM image of the Pd/MIL-100(Cr) sample and its corresponding particle size distribution. The size distribution is counted by the software of particle size analysis according to the TEM image. (b) HRTEM image of the Pd/MIL-100(Cr) sample. (c) Dark-field STEM image of the Pd/MIL-100(Cr) sample. (d) Corresponding elemental mapping with Pd in the red rectangle of part c. The white circles represent Pd NPs. (e) EDX spectrum of the Pd/MIL-100(Cr) sample. (f) ESR spectrum of pure Pd NPs. Pure NPs are the samples before the introduction of MIL-100(Cr).

the SI reveals typical scanning electron microscopy (SEM) and transmission electron microscopy (TEM) images of the MIL-100(Cr) sample. Especially, the SEM image (Figure S2a in the SI) implies that the sample consisted of small octahedral structures (the inset of Figure S2a in the SI), and the TEM image (Figure S2c in the SI) reveals that a single MIL-100(Cr) is nearly spherical with a diameter of about 1 μm. Because of its micron-scale dimension, the surface effect of this material can be neglected, which allows the surface effect of Pd NPs to be carefully investigated without interference. From the TEM image and its corresponding cumulative grain size distribution (Figure 1a), it can be clearly seen that Pd NPs are highly dispersed on MIL-100(Cr) structures, and their size distributions are determined to be 5.4 ± 0.7 nm. The distribution of Pd atoms in MIL-100(Cr) was further determined by high-angle annular dark-field scanning TEM (HAADF-STEM)—energy-dispersive X-ray (EDX) spectroscopy. The high-resolution TEM (HRTEM) image (Figure 1b) reveals that the lattice spacing of 0.230 nm can be assigned to the (111) plane of Pd NPs. Dark-field STEM (Figure 1c) and EDX mapping (Figure 1d) of Pd NPs further show the existence and distribution of Pd NPs. In the EDX spectrum (Figure 1e), except the Cu element from a Cu foil, the other elements including C, O, and metal center Cr from the MIL-100(Cr) structure and the Pd element can all be detected.

The catalytic performance of Pd/MIL-100(Cr) was characterized using liquid-phase reduction of 4-NP to 4-AP by $NaBH_4$ as a model reaction system. When Pd/MIL-100(Cr) NC was added to the solution, the absorption of 4-NP at 400 nm decreased along with a concomitant increase of the 300 nm

DOI: 10.1021/am509218a
ACS Appl. Mater. Interfaces 2015, 7, 6019−6024

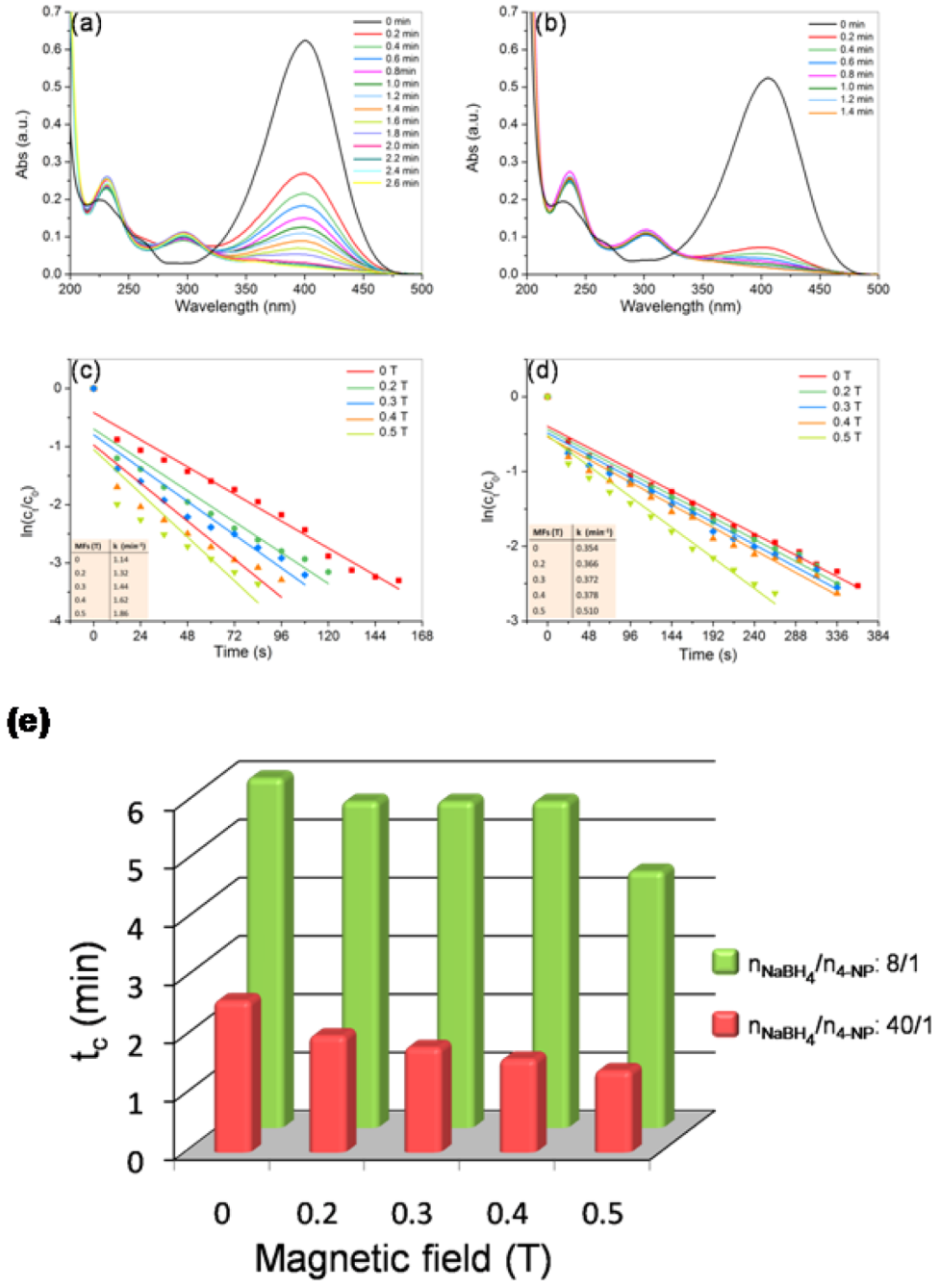

Figure 2. Variation in UV−vis absorption spectra at 0.2 min intervals for 4-NP reduction reaction in Pd/MIL-100(Cr) NCs without (a) and with a 0.5 T MF (b). Plot of $\ln(c_t/c_0)$ of 4-NP against time for Pd/MIL-100(Cr) NCs under different MF intensities from about 0, 0.2, 0.3, 0.4 to 0.5 T. The relationship between the MFs and k values is shown in the bottom left corner with [4-NP] = 3×10^{-2} mol L^{-1}, [$NaBH_4$] = 3×10^{-1} mol L^{-1}, and [Pd/MIL-100(Cr)] = 1 mg (c) and [4-NP] = 3×10^{-2} mol L^{-1}, [$NaBH_4$] = 6×10^{-2} mol L^{-1}, and [Pd/MIL-100(Cr)] = 1 mg (d). (e) Time for completion for the reaction (t_c) reduced with an increase of the MF intensity from 0, 0.2, 0.3, 0.4 to 0.5 T.

peak of 4-AP, respectively (Figure 2a). The complete reduction of 4-NP was achieved within 3 min over the catalysts of Pd/MIL-100(Cr), while the reaction time was much shorter if a MF was applied to the reaction system (Figures 2b and S3 in the SI). From Figure S4 in the SI, it can be seen that the catalytic rate was very fast at the initial period t_0. The reduction reaction could be reasonably assumed as a pseudo-first-order reaction from t_0 with regard to 4-NP only. This pseudo-first-order kinetics can be written as $\ln(c_t/c_0) = -kt$, where k is the kinetic rate constant, c_t and c_0 are the apparent and initial concentrations of 4-NP, respectively, and t is the time of real-time reaction. A rapid and almost linear evolution can be observed between t and $\ln(c_t/c_0)$. The values of kinetic rate constant (k) can be calculated from the slope. The results also show that t_c (the time of completion for the reaction) is gradually reduced from 2.6, 2.0, 1.8, 1.6 to 1.4 min with an increase of the MF intensity from about 0, 0.2, 0.3, 0.4 to 0.5 T (see Figure 2e). Significantly, the k value of the catalytic reaction without a MF applied is calculated to be 1.08 min^{-1}, which is slightly lower than that under MFs (see the inset of Figure 2c). As the intensity of the MF reached 0.5 T, the k value was about 1.13 min^{-1}. This indicates that MFs can

DOI: 10.1021/am509218a
ACS Appl. Mater. Interfaces 2015, 7, 6019−6024

Scheme 1. Schemes of (a) 4-NP Molecules Adsorbed at the Surface of MIL-100(Cr) and (b) 4-NP Reduction at the Surface of Pd NPs without (i) and with (ii) MFs[a]

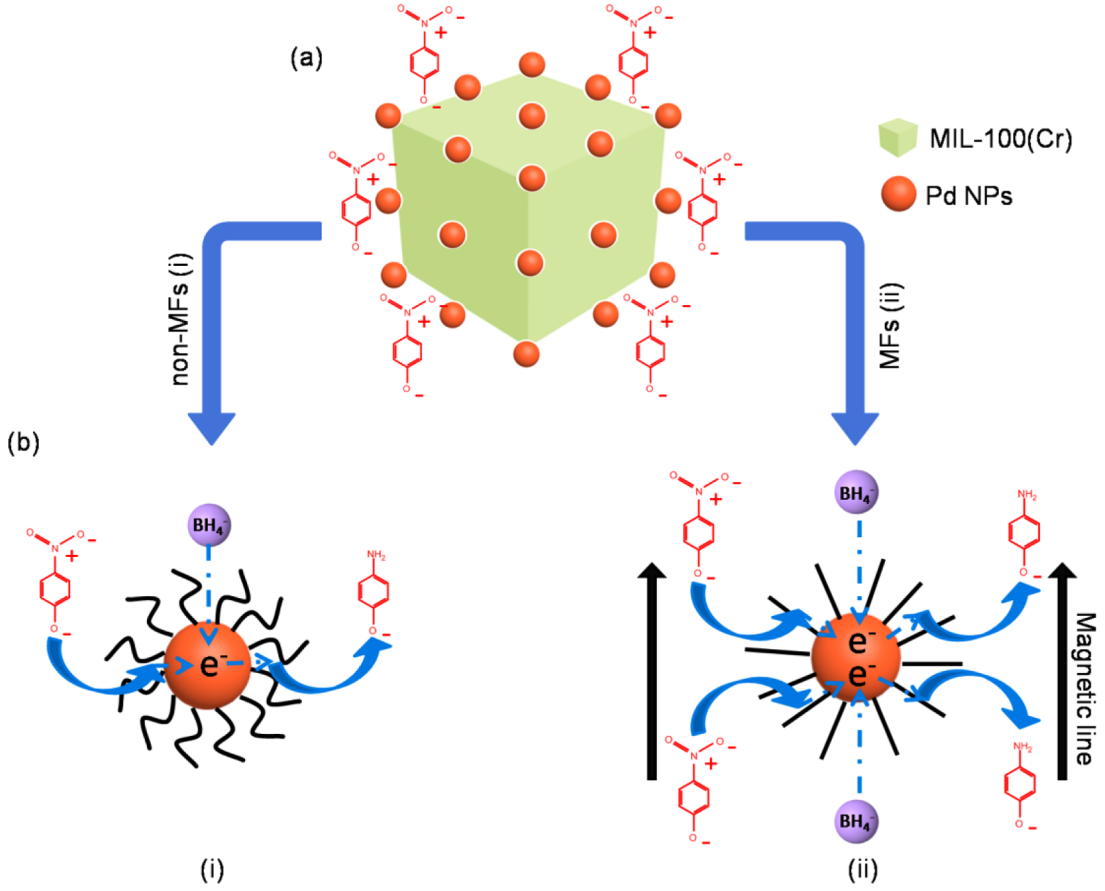

[a]When an external MF was introduced, the spin arrangement changed from disordered (i) to ordered (ii) configuration, accompanied by increasing adsorption of the reactant 4-NP and desorption of the product 4-AP.

improve the reduction rate of 4-NP and shorten its reduction time. The k value (1.13 min^{-1}) is superior to many other metal-based catalysts under ambient conditions [e.g., 0.3 min^{-1} for Au@Ag/ZIF-8,[18] 0.33 min^{-1} for Au/MIL-100(Fe),[19] and 0.632 min^{-1} for Pd NPs/CNT-220[20]]. Next, we also performed experiments with the concentration of $NaBH_4$ changed from 40 to 8 times. The reduction of 4-NP under different MF intensities can be seen as above. As shown in Figure 2d, with an increase of the MF intensity from about 0, 0.2, 0.3, 0.4 to 0.5 T, t_c gradually was reduced from 6.0, 5.6, 5.6, 5.6 to 4.4 min (see Figure 2e). Significantly, the k value was calculated as 0.330 min^{-1}, which is slightly lower than the reaction carried out under MFs (see the inset of Figure 2d). When the MF intensity reached 0.5 T, the k value became 0.464 min^{-1}. Here, the enhancement effect of MFs on the reduction rate of 4-NP can be well confirmed. According to Arrhenius' equation, it was calculated that the activation energy under 0.5 T was reduced by 0.11 kJ mol^{-1} relative to that without MFs applied (details can be seen in the SI), implying that MFs favor the formation of the transition state of 4-NP molecules on the surface of Pd catalysts.

From the results shown above, one can clearly observe that the catalytic activity of Pd/MIL-100(Cr) under a MF is higher than that without a MF and gradually increased along with an increase in the MF intensity. In Pd-supported MIL-100(Cr) composite materials, the catalytic activity can be attributed to the synergistic effect of Pd and MIL-100(Cr), similar to those reported in the literature.[21,22] The mechanism may be explained as follows: first, 4-NP molecules were adsorbed onto mesoporous MIL-100(Cr) structures via $\pi-\pi$-stacking interactions between the aromatic rings of 4-NP and the organic ligands of MIL-100(Cr) and via interactions between the hydroxyl groups of 4-NP and the Cr^{2+} metal center in the framework. As shown in Scheme 1a, the adsorption of 4-NP onto MIL-100(Cr) gives rise to a local high concentration of 4-NP, which increases the contact probability of 4-NP molecules on the surface of Pd NPs and thus enhances the catalytic efficiency of 4-NP reduction. Then electron transfer takes place from BH_4^- to Pd NPs and subsequently 4-NP molecules adsorbed on Pd NPs take electrons (see Scheme 1b). In this study, the size of the Pd NPs is about 5 nm. As seen in Figure 1f, the ESR spectrum of pure Pd NPs displays the main peak near 337 mT. The ESR signal, with g = 1.92, is typical of paramagnetic Pd NPs, which indicates that Pd NPs are paramagnetic because of uncanceled surface spins. The adsorption of 4-NP on the surface of Pd NPs is closely related with the spin arrangement. When an external MF is introduced, the surface spin configuration of Pd NPs will change from paramagnetic to ferromagnetic.[23] The change of the configuration would affect the adsorption of 4-NP on the surface of Pd NPs, inevitably inducing changes of the adsorption number of 4-NP molecules on the surface of the catalyst.

For understanding the effect of MFs on the catalytic activity, theoretical calculations of the adsorption energy of 4-NP

DOI: 10.1021/am509218a
ACS Appl. Mater. Interfaces 2015, 7, 6019−6024

molecules on the surface of Pd NPs with a MF applied were carried out (calculation details can be seen in the SI). The (111) surface is chosen as the optimizing model based on HRTEM results (see Figure 1b). In this condition, the introduction of MFs into the model was simulated by using the models with different configurations, one with a paramagnetic-like configuration (Scheme S1 in the SI) and the other with a ferromagnetic-like configuration (Scheme S1b in the SI). In the absence of MFs, spins on the Pd surface arrange in a disordered manner, corresponding to a paramagnetic-like configuration and showing no spin-charge distribution (Figure 3a). However, when a MF is applied, the Pd atoms near the

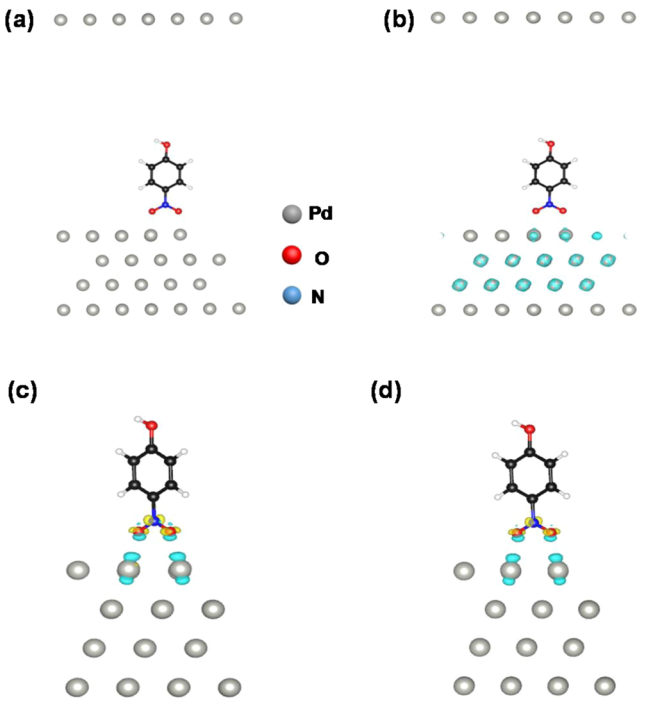

Figure 3. Total spin-polarized charge density of 4-NP adsorbed on the Pd(111) surface without (a) and with (b) MFs. The blue region refers to the isosurface value of 0.2 e Å^{-3}. Charge-density difference of 4-NP adsorbed on the Pd(111) surface without (c) and with (d) MFs. The isosurface value of the color region is 0.08 e Å^{-3}. The yellow and blue regions refer to positive and negative charge distributions, respectively.

(111) surface are magnetized and spins align parallel, corresponding to a ferromagnetic-like configuration and showing spin-charge distribution (Figure 3b). The method had also been proven to be reasonable in our previous study.[17] Next, we optimized and calculated different structures and adsorption energies of 4-NP on various adsorption sites of the Pd(111) surface. Through three kinds of calculations (calculation details can be seen in the SI), it can be concluded that 4-NP molecules were adsorbed on the bridge site of the Pd(111) surface via the O atoms in the nitro groups (see Scheme S1a,b in the SI). This adsorption geometry is similar to the structure of 4-NP adsorbed on the bimetallic dendrimer-encapsulated NPs.[24] The charge-density difference of 4-NP adsorbed on the surface of Pd NPs without and with MFs can be seen in parts c and d of Figure 3, respectively. The results show that their difference is almost negligible. Also, the change of the charge density only takes place in the region between the adsorbate and substrate, indicating that there is a contribution from covalent binding during the adsorption process.

Table S1 in the SI shows the calculated energy of 4-NP adsorbed on the surface of Pd NPs through the O atoms of the nitro group on the bridge site with and without MFs. It can be seen that both the energy of the clean Pd surface and the total adsorption system were decreased under MFs (−177.52 and −276.36 eV, respectively) compared to those without MFs applied (−177.28 and −276.20 eV, respectively). The calculation results show that MFs can effectively reduce the total energy of the adsorption system. Furthermore, Raman spectra (Figure S5 in the SI) also show that NO_2 peaks at 1560, 1389, and 659 cm^{-1} under a 0.5 T MF (ii) are slightly stronger than those without a MF applied (i), implying that MFs can increase the adsorption number of 4-NP molecules on the surface of Pd catalysts. Interestingly, the adsorption energy (ΔE_{ads}) of the system with MFs (−0.33 eV) is a little higher than that without MFs (−0.41 eV). However, ΔE_{ads} in both cases is very small, which indicates that this type of bonding is rather weak. Therefore, the adsorption and desorption energy of 4-NP molecules from the surface of the catalysts is not the decisive factor for the reaction rate. In addition, the structure and energy of 4-AP adsorbed on the Pd(111) surface were also optimized and calculated (see Scheme S2 in the SI). The optimized structure is similar to 4-NP adsorbed on the bridge site of the Pd(111) surface illustrated in Scheme S1 in the SI. The amino group is a little far away from the Pd surface compared with the nitro group, with approximately 3 Å. The calculation shows that the adsorption energy of the amino group (−0.170 and −0.159 eV performed without and with MFs, respectively) is also weaker than that of the nitro group, indicating that the adsorption/desorption energy of the product (4-AP) should not be a determining factor. It is therefore suggested that the reaction rate is determined by the adsorption number of 4-NP molecules.

Preparing NCs with smaller sizes and high-index facets is the general way to make further improvements to the catalytic performance. However, when these NCs have been prepared, their activity will remain constant or decrease with time. Here, it is found that the catalytic activity of Pd NCs can be effectively improved by magnetization of their surface spins. As we know, all NPs usually have plenty of surface spins, and the spins are canted or disordered. For example, the surface spin of Co NPs with diameters of 1.6 nm can account for 60% of the total spins.[25] Under the induction of MFs, these spin arrangements can change from disordered to ordered; accordingly, the catalytic performance of NPs will be responsive to this change, such as showing a catalytic activity that can be switched on and off when the intensity of the MF is changed. Then, a chemical reaction catalyzed by certain NPs can be induced or sped up by altering the strength of an applied MF, which is highly valuable in the chemical industry. In addition, it is expected that an increase in the MF intensity (>0.5 T) may further lower the activation energy, leading to more types of NPs as catalysts, and the catalyzed reaction proceeds at a quicker rate.

The effect of MFs on the reduction of 4-NP using Pd/MIL-100(Cr) as catalysts was studied systemically. The experimental results show that MFs can increase the reaction rate (1.13 min^{-1}) and decrease the activation energy. The theoretical results demonstrate that the surface spin configuration of Pd NPs changing from paramagnetic to ferromagnetic as induced by MFs would decrease the energy of the total adsorption system, favorable for the adsorption number of 4-NP molecules

DOI: 10.1021/am509218a
ACS Appl. Mater. Interfaces 2015, 7, 6019−6024

onto the surface of the catalysts. It is hopeful that the study can help us gain a better understanding of the change of the surface spin arrangement of the NC under MFs and provide guidance for the development of external MFs as a tool for regulating the activities of NCs.

■ ASSOCIATED CONTENT

Supporting Information

Experimental section, sample characterization methods, and details of theoretical calculations, XRD, SEM, and UV−vis spectra, Raman data, and a video of the actual process of 4-NP reduction. This material is available free of charge via the Internet at http://pubs.acs.org.

■ AUTHOR INFORMATION

Corresponding Author

*E-mail: cqw@ustc.edu.cn. Fax and Tel: +86 551 63603005.

Author Contributions

†R.L. and Y.Y. contributed equally to this research.

Notes

The authors declare no competing financial interest.

■ ACKNOWLEDGMENTS

Financial support from the National Natural Science Foundation of China (Grants 21271163 and U1232211) and Collaborative Innovation Center of Suzhou Nano Science and Technology is gratefully acknowledged. The calculations were completed on the supercomputing system in the Supercomputing Center of USTC.

■ REFERENCES

(1) Wang, Y. H.; Wang, F.; Song, Q.; Xin, Q.; Xu, S. T.; Xu, J. Heterogeneous Ceria Catalyst with Water-Tolerant Lewis Acidic Sites for One-Pot Synthesis of 1,3-Diols via Prins Condensation and Hydrolysis Reactions. *J. Am. Chem. Soc.* **2013**, *135*, 1506−1515.

(2) Cheng, C.; Kim, B. G.; Guironnet, D.; Brookhart, M.; Guan, C. J.; Wang, D. Y.; Krogh-Jespersen, K.; Goldman, A. S. Synthesis and Characterization of Carbazolide-Based Iridium PNP Pincer Complexes. Mechanistic and Computational Investigation of Alkene Hydrogenation: Evidence for an Ir(III)/Ir(V)/Ir(III) Catalytic Cycle. *J. Am. Chem. Soc.* **2014**, *136*, 6672−6683.

(3) Fihri, A.; Bouhrara, M.; Nekoueishahraki, B.; Basset, J. M.; Polshettiwar, V. Nanocatalysts for Suzuki Cross-Coupling Reactions. *Chem. Soc. Rev.* **2011**, *40*, 5181−5203.

(4) Mlynarski, S. N.; Schuster, C. H.; Morken, J. P. Asymmetric Synthesis from Terminal Alkenes by Cascades of Diboration and Cross-Coupling. *Nature* **2014**, *505*, 386−390.

(5) Zou, X. X.; Goswami, A.; Asefa, T. Efficient Noble Metal-Free (Electro)Catalysis of Water and Alcohol Oxidations by Zinc−Cobalt Layered Double Hydroxide. *J. Am. Chem. Soc.* **2013**, *135*, 17242−17245.

(6) Wang, X.; Liu, D. P.; Song, S. Y.; Zhang, H. J. Pt@CeO_2 Multicore@Shell Self-Assembled Nanospheres: Clean Synthesis, Structure Optimization, and Catalytic Applications. *J. Am. Chem. Soc.* **2013**, *135*, 15864−15872.

(7) Tsao, Y. C.; Rej, S.; Chiu, C. Y.; Huang, M. H. Aqueous Phase Synthesis of Au−Ag Core−Shell Nanocrystals with Tunable Shapes and Their Optical and Catalytic Properties. *J. Am. Chem. Soc.* **2014**, *136*, 396−404.

(8) Dhakshinamoorthy, A.; Garcia, H. Catalysis by Metal Nanoparticles Embedded on Metal−Organic Frameworks. *Chem. Soc. Rev.* **2012**, *41*, 5262−5284.

(9) MacMillan, D. W. C. The Advent and Development of Organocatalysis. *Nature* **2008**, *455*, 304−308.

(10) Zeng, H. C. Integrated Nanocatalysts. *Acc. Chem. Res.* **2013**, *46*, 226−235.

(11) Zhang, H.; Jin, M. S.; Xiong, Y. J.; Lim, B.; Xia, Y. N. Shape-Controlled Synthesis of Pd Nanocrystals and Their Catalytic Applications. *Acc. Chem. Res.* **2013**, *46*, 1783−1794.

(12) Li, Y.; Shen, W. J. Morphology-Dependent Nanocatalysts: Rod-Shaped Oxides. *Chem. Soc. Rev.* **2014**, *43*, 1543−1574.

(13) Han, Y. F.; Kumar, D.; Goodman, D. W. Particle Size Effects in Vinyl Acetate Synthesis over Pd/SiO_2. *J. Catal.* **2005**, *230*, 353−358.

(14) Tian, N.; Zhou, Z. Y.; Sun, S. G.; Ding, Y.; Wang, Z. L. Synthesis of Tetrahexahedral Platinum Nanocrystals with High-Index Facets and High Electro-Oxidation Activity. *Science* **2007**, *316*, 732−735.

(15) Chen, C. P.; Chen, Y. J. Liquid-Phase Synthesis of 2-Substituted Benzimidazoles, Benzoxazoles and Benzothiazoles. *Tetrahedron Lett.* **2004**, *45*, 113−115.

(16) Teranishi, T.; Hori, H.; Miyake, M. ESR Study on Palladium Nanoparticles. *J. Phys. Chem. B* **1997**, *101*, 5774−5776.

(17) Wang, M. S.; Chen, Q. W. Experimental and Theoretical Investigations on the Magnetic-Field-Induced Variation of Surface Energy of Co_3O_4 Crystal Faces. *Chem.—Eur. J.* **2010**, *16*, 12088−12090.

(18) Jiang, H. L.; Akita, T.; Ishida, T.; Haruta, M.; Xu, Q. Synergistic Catalysis of Au@Ag Core−Shell Nanoparticles Stabilized on Metal−Organic Framework. *J. Am. Chem. Soc.* **2011**, *133*, 1304−1306.

(19) Ke, F.; Zhu, J. F.; Qiu, L. G.; Jiang, X. Controlled Synthesis of Novel Au@MIL-100(Fe) Core−Shell Nanoparticles with Enhanced Catalytic Performance. *Chem. Commun.* **2013**, *49*, 1267−1269.

(20) Gu, X. M.; Qi, W.; Xu, X. Z.; Sun, Z. H.; Zhang, L. Y.; Liu, W.; Pan, X. L.; Su, D. S. Covalently Functionalized Carbon Nanotube Supported Pd Nanoparticles for Catalytic Reduction of 4-Nitrophenol. *Nanoscale* **2014**, *6*, 6609−6616.

(21) Gu, X. J.; Lu, Z. H.; Jiang, H. L.; Akita, T.; Xu, Q. Synergistic Catalysis of Metal−Organic Framework-Immobilized Au−Pd Nanoparticles in Dehydrogenation of Formic Acid for Chemical Hydrogen Storage. *J. Am. Chem. Soc.* **2011**, *133*, 11822−11825.

(22) Jiang, H. L.; Akita, T.; Ishida, T.; Haruta, M.; Xu, Q. Synergistic Catalysis of Au@Ag Core−Shell Nanoparticles Stabilized on Metal−Organic Framework. *J. Am. Chem. Soc.* **2011**, *133*, 1304−1306.

(23) Reddy, B. V.; Khanna, S. N.; Dunlap, B. I. Giant Magnetic Moments in 4d Clusters. *Phys. Rev. Lett.* **1993**, *70*, 3323−3326.

(24) Pozun, Z. D.; Rodenbusch, S. E.; Keller, E.; Tran, K.; Tang, W. J.; Stevenson, K. J.; Henkelman, G. A Systematic Investigation of *p*-Nitrophenol Reduction by Bimetallic Dendrimer Encapsulated Nanoparticles. *J. Phys. Chem. C* **2013**, *117*, 7598−7604.

(25) Xavier, B.; Amilcar, L. Finite-Size Effects in Fine Particles: Magnetic and Transport Properties. *J. Phys. D: Appl. Phys.* **2002**, *35*, R15−R42.

(26) Férey, G.; Serre, C.; Mellot-Draznieks, C.; Millange, F.; Surblé, S.; Dutour, J.; Margiolaki, I. A Hybrid Solid with Giant Pores Prepared by a Combination of Targeted Chemistry, Simulation, and Powder Diffraction. *Angew. Chem.* **2004**, *116*, 6456.

DOI: 10.1021/am509218a
ACS Appl. Mater. Interfaces 2015, 7, 6019−6024